

## Developing Fe<sub>3</sub>O<sub>4</sub> nanoparticles into an efficient multimodality imaging and therapeutic probe

Cite this: *Nanoscale*, 2013, 5, 11954

Rui Hao,<sup>a</sup> Jing Yu,<sup>a</sup> Zigang Ge,<sup>b</sup> Lingyun Zhao,<sup>\*c</sup> Fugeng Sheng,<sup>d</sup> Lili Xu,<sup>d</sup> Gongjie Li<sup>d</sup> and Yanglong Hou<sup>\*a</sup>

A rapid ligand-exchange method was developed to transfer high quality hydrophobic magnetite nanocrystals into water-soluble NPs by using protocatechuic acid as a ligand *via* homogenous reaction. After ligand exchange, the magnetite nanocrystals not only exhibited outstanding stability in water, but also maintained high crystallinity and saturation magnetization. Cell viability experiments demonstrated good biocompatibility of the NPs. For 12 nm magnetite nanoparticles (NPs), the small hydrodynamic size of 14 nm enabled a high  $T_1$  relaxivity of  $17.8 \text{ mM}^{-1} \text{ s}^{-1}$  while high saturation magnetization of  $77.8 \text{ emu g}^{-1}$  enabled the NPs to exhibit a high  $T_2$  relaxivity of  $220 \text{ mM}^{-1} \text{ s}^{-1}$  in MRI phantom experiments. *In vivo* MR imaging experiments further confirmed that the NPs were eminent  $T_1$  and  $T_2$  contrast agents. Moreover, the high quality NPs can be used as excellent magnetic heating agents under an alternating magnetic field. With all those features, including multimodality imaging and magnetic hyperthermia, the NPs can be used as single compound multifunctional agents for various biomedical applications, especially for cancer diagnosis and therapy.

Received 7th August 2013

Accepted 27th September 2013

DOI: 10.1039/c3nr04157c

[www.rsc.org/nanoscale](http://www.rsc.org/nanoscale)

### Introduction

Multifunctional nanoparticles are intensively studied for multimode imaging or disease theranostics, especially for cancer.<sup>1</sup> Among the various diagnostic methods, magnetic resonance imaging (MRI) is one of the most powerful non-invasive, real-time means, with high spatial resolution.<sup>2,3</sup> According to different types of relaxation times,  $T_1$ - or  $T_2$ -weighted images can be obtained using MRI. The former shows the anatomic structure of soft-tissue, while the latter indicates pathological changes. It will be more powerful to diagnose diseases by combining the two complimentary modes.<sup>4,5</sup> Commonly,  $T_1$ -weighted images could be enhanced by using  $T_1$  contrast agent complexes or nanoparticles (NPs) with paramagnetic ions including Fe<sup>3+</sup>, while ferromagnetic and superparamagnetic NPs are selected as  $T_2$  contrast agents.<sup>6</sup> Dual contrast mode enhancement by a single contrast agent is one of the most promising subjects in the area.<sup>4,7,8</sup> Generally, the higher the ratio of  $r_2/r_1$ , the better the efficiency of a  $T_2$  contrast agent, and *vice versa* for a  $T_1$  contrast agent.<sup>9</sup> Specifically, for a  $T_1$

contrast agent, the  $r_2/r_1$  should be in the range of 1–2, while for a  $T_2$  contrast agent, it should be higher than 10. Between 2 and 10, the contrast agent can work as both a  $T_1$  and  $T_2$  contrast agent.<sup>10,11</sup> Moreover, multifunctional nanoparticles are intensively studied for the purpose of multimodality imaging or cancer theranostics. Particularly, using magnetic materials as heating agents upon exposure under an alternating magnetic field (AMF) as a heating source can be a very effective method for cancer treatment.<sup>12</sup> It is very likely to use magnetic NPs (MNPs) as single-compound multifunctional agents for both of  $T_1$  and  $T_2$  imaging as well as cancer hyperthermia. Although the combination of  $T_2$  imaging and magnetic hyperthermia was reported,<sup>13</sup> there are very few reports on the MNPs exhibiting those three features in a single platform.

Magnetite with high magnetization up to  $92 \text{ emu g}^{-1}$  and no toxic element such as Co, Mn and Ni, has shown great potential as a  $T_1$  or  $T_2$  MRI contrast agent under different circumstances.<sup>14–17</sup> As good  $T_1$ -weighted MRI contrast agents, the distance between paramagnetic ions and the water phase should be very short.<sup>18</sup> To endow iron oxide NPs high longitudinal relaxivity, several pivotal parameters, including small particle size, thin coating layer and good water solubility should be achieved. On the other hand, both the transverse relaxivity<sup>19</sup> and the specific absorption rate (SAR)<sup>20,21</sup> of the MNPs are proportional to the square of their saturation magnetization. Hence, for  $T_2$ -weighted MRI contrast agents and magnetic hyperthermia application, the magnetic performance of Fe<sub>3</sub>O<sub>4</sub> should be systematically studied, and high saturation magnetization is preferred.<sup>19,22,23</sup>

<sup>a</sup>Department of Materials Science and Engineering, College of Engineering, Peking University, Beijing 100871, China. E-mail: [houl@pku.edu.cn](mailto:houl@pku.edu.cn)

<sup>b</sup>Department of Biomedical Engineering, College of Engineering, Peking University, Beijing 100871, China

<sup>c</sup>Institute of Medical Physics, Key Laboratory of Particle & Radiation Imaging, Ministry of Education, Department of Engineering Physics, Tsinghua University, Beijing, China. E-mail: [nuszly@gmail.com](mailto:nuszly@gmail.com)

<sup>d</sup>Department of Radiology, Affiliated Hospital of the Academy of Military Medical Sciences, China

Several protocols, such as precipitation or polyol-mediated synthesis have been reported for the fabrication of hydrophilic MNPs. Despite the good solubility and thin coating layer, MNPs prepared using these protocols normally possess magnetic moment below  $50 \text{ emu g}^{-1}$ . In contrast, high quality  $\text{Fe}_3\text{O}_4$  with high crystallinity, controlled morphology, narrow size-distribution and high magnetic moment, which is synthesized by a thermo-decomposition or solvothermal method, is usually hydrophobic, due to the long-chain hydrocarbon surfactants employed in the synthetic process.<sup>24–26</sup> Moreover, as  $T_1$  contrast agents, the aggregation of  $\text{Fe}_3\text{O}_4$  NPs would compromise the contrast effect. Therefore, excellent water solubility of high quality NPs for avoiding magnetic induced aggregation is essential for single compound dual-mode contrast agents.

Lots of efforts have been made to obtain high quality  $\text{Fe}_3\text{O}_4$  NPs with good water solubility. The addition of amphiphilic molecules may be one effective strategy to get hydrophilic NPs.<sup>22</sup> However, it will prolong the distance between NPs and water, and decrease the  $T_1$  MRI signal. For shorter distance from the water phase to the surface of nanoparticles, direct exchange of the original surfactants into hydrophilic ones is preferred. Plenty of successful ligand-exchange strategies have been developed for preparation of water soluble MNPs.<sup>23–31</sup> Generally, new ligands always consist of two key parts: the linkage group and hydrophilic group. Carboxyl,<sup>23</sup> mercapto,<sup>32</sup> silane,<sup>29</sup> phosphate<sup>33</sup> and catechol groups<sup>34,35</sup> are usually selected as linkage groups. Strong interaction between the linkage group and the surface of MNPs will allow the occurrence of ligand-exchange. Among the widely used stabilizers, catechol-derivatives have been intensively explored as linkage groups due to high affinity to metal oxides and good biocompatibility.<sup>36</sup> On the other side, despite the abundant choices of linkage groups, the hydrophilic groups for ligand-exchange are limited to few options such as polyethylene glycol (PEG),<sup>15,33,37</sup> carboxyl group,<sup>38</sup> zwitterionic dopamine sulfonate<sup>39</sup> and phosphonate modified sugar molecules.<sup>19</sup> However, long ligand exchange time, non-commercially available ligands and inert atmosphere for reaction may limit the further application of these protocols. Moreover, few MNPs by these methods can be applied for dual-mode MRI contrast agent. Therefore, it is highly needed to find a rapid, facile method for the preparation of high quality MNPs with excellent water-solubility and biocompatibility for multifunctional applications.

In this paper, we developed a new ligand-exchange strategy to rapidly prepare functional MNPs for dual-mode MR contrast and magnetic hyperthermia. Protocatechuic acid (PA) was employed as the novel ligand and hydrophobic MNPs can be transferred into hydrophilic ones within 15 min. The 12 nm PA stabilized iron oxide NPs (PAIONs) can be readily dispersed in water and phosphate buffer solution (PBS) with very small hydrodynamic size of 14 nm, which is similar to the results of pristine NPs observed by TEM. The concentration of PAIONs in water can reach up to  $10 \text{ mg mL}^{-1}$  and the solution shows the characteristics of magnetic ferrofluids. The 12 nm PAIONs exhibited superparamagnetic behavior with saturation magnetization up to  $77.8 \text{ emu g}^{-1}$ . Both high  $r_1$  and  $r_2$  relaxivities of  $17.8 \text{ mM}^{-1} \text{ s}^{-1}$  and  $220 \text{ mM}^{-1} \text{ s}^{-1}$  as well as satisfactory

biocompatibility can be confirmed. The *in vivo* MRI results demonstrated that the PAIONs could be high performance dual-mode contrast agents both for  $T_1$  and  $T_2$ -weighted MR imaging. Inductive heating property of the PAIONs was confirmed by exposing the magnetic colloidal liquid under the AMF. Combining the above mentioned properties, PAIONs reported here can further be used as dual-mode MRI contrast/magnetic hyperthermia single compound multifunctional agents.

## Experimental

### Materials

Iron(III) acetylacetonate ( $\text{Fe}(\text{acac})_3$ , 99.9%) was purchased from Yili Chemicals. Iron carbonyl (99%) and oleyl amine were purchased from Xindingpengfei Chemicals. Oleic acid (OA, 90%), protocatechuic acid (PA, 99.9%), and 1-octadecene (ODE, 90%) were purchased from Alfa Aesar.

### Synthesis of MNPs

In a typical synthesis of 12 nm OA-stabilized MNPs, 1 mmol of  $\text{Fe}(\text{acac})_3$  was added into 20 mL ethanol solution containing 1.2 mL of OA. The mixture solution was stirred for 10 min and transferred to a steel-lined Teflon autoclave of 25 mL. The autoclave was then sealed and kept at  $180 \text{ }^\circ\text{C}$  for 12 h. After cooling down to room temperature, the precipitate was collected. Excess ethanol was added into the solution and the NPs could be collected by centrifugation (10 000 rpm, 5 min).

5 nm OA-stabilized MNPs were prepared as described previously with a little modification.<sup>24</sup> The standard Schlenk line technique, which was carried out under an argon atmosphere, was used. 2 mmol of iron carbonyl was injected into a mixture containing 2 mL of OA and 20 mL of ODE at room temperature. The solution was heated to  $310 \text{ }^\circ\text{C}$  at a heating rate of  $5 \text{ }^\circ\text{C min}^{-1}$  and kept at this temperature for 30 min. After the solution cooled down to room temperature, excess isopropanol was added and the NPs could be collected by centrifugation (10 000 rpm, 10 min).

25 nm OAm-stabilized MNPs were prepared according to our previous report.<sup>40</sup> Typically, 1 mmol of  $\text{Fe}(\text{acac})_3$  was added into 20 mL toluene solution containing 5 mL of OAm. The mixture solution was stirred for 10 min and transferred to a steel-lined Teflon autoclave of 25 mL. Then the autoclave was sealed and kept at  $200 \text{ }^\circ\text{C}$  for 24 h. 20 mL of ethanol was added in to the solution and the NPs could be collected by centrifugation (10 000 rpm, 5 min). MNPs with various sizes as prepared by the above mentioned methods were dissolved in toluene for further experiments.

### Ligand-exchange reaction

0.4 g PA was first dissolved in the mixture of 1 mL pyridine and 3 mL toluene. Then the solution was added dropwise into 100 mL of the toluene solution containing 100 mg MNPs. With the addition of PA solution, the MNPs precipitated immediately. The precipitate was then dissolved in sodium carbonate solution (1%, w/v, 10 mL). Excess ethanol was added in to the solution and the MNPs could be collected by centrifugation

(10 000 rpm, 1 min). The MNPs would be dissolved in water again, precipitated by ethanol and collected by centrifugation (10 000 rpm, 1 min) for washing the NPs. Then the resulting MNPs can be easily dissolved in water or PBS solution by hand shaking.

### Characterizations

The basic characterization of MNPs before and after ligand-exchange was carried out by transmission electron microscopy (TEM), X-ray diffraction (XRD), X-ray photoelectron spectroscopy (XPS), fourier transform infrared spectroscopy (FTIR), magnetic property measurement system (MPMS), physical property measurement system (PPMS), dynamic light scattering (DLS) and thermogravimetric analysis (TGA). TEM images were obtained with FEI Tecnai F20 microscopy operated at 200 kV. Powder XRD patterns were obtained with a Rigaku DMAX-2400 X-ray diffractometer equipped with Cu K $\alpha$  radiation and the accelerating voltage and current were 40 kV and 300 mA. XPS measurements were performed on an Axis Ultra (Kratos Analytical Ltd.) imaging photoelectron spectrometer using a monochromatized aluminum K $\alpha$  anode, and the C1s peak at 284.8 eV was taken as an internal standard. ATR-FTIR spectra were measured using a VECTOR 22 Nicolet spectrometer. The magnetic property of the NPs was investigated on MPMS or PPMS (Quantum Design). DLS was tested using a Zeta PALS particle size analyzer (Brookhaven Instrument). TGA results were recorded on a Q50TGA (Thermal Analysis) under a N<sub>2</sub> atmosphere and the samples were heated to 600 °C at 10 °C min<sup>-1</sup> to determine the amount of pure iron oxide and surfactant. The concentration of Fe<sup>3+</sup> was quantified using an inductively coupled plasma-atomic emission spectrometer (ICP-AES, PROFILE SPEC, Leeman).

### Measurement of MRI relaxation properties

$T_1$  and  $T_2$  relaxation of the aqueous solutions with various concentrations of PAIONs were measured in test tubes with a 1.5 T clinical MRI scanner (Signa EXCITE HD 1.5 T Twinspeed system, General Electric Company, USA). MR images were acquired using a  $T_1$ -weighted sequence with the following parameters: repetition time (TR) = 300, 350, 400, 450, 500, 550, 600, 650 ms, echo time (TE) = 11 ms, matrix size = 256 × 256, field of view (FOV) = 120 × 120 mm<sup>2</sup>, slice thickness = 2 mm, NEX = 1. The parameters of a  $T_2$ -weighted sequence were as follows: TR = 3000 ms, TE = 0, 30, 40, 60, 80, 100, 120, 140 ms, matrix size = 256 × 256, field of view (FOV) = 120 × 120 mm<sup>2</sup>, slice thickness = 2 mm, and NEX = 1. All post-processings were performed on the GE ADW 4.3 workstation.  $T_1$ -mapping and  $T_2$ -mapping images were acquired by using the post-processing software of research in Functool. The selected region of interests (ROIs) in the  $T_1$ -mapping and  $T_2$ -mapping was measured with the same size to obtain the signal intensities for each concentration. Based on the inverse relaxation time ( $1/T_1$ ) and ( $1/T_2$ ), the resulting  $r_1$  and  $r_2$  values were measured *versus* Fe<sup>3+</sup> concentrations.

### Cell viability

All cell culture related reagents were purchased from Invitrogen. HeLa cells were obtained from Cancer Institute and Hospital, Chinese Academy of Medical Science. HeLa cells were first seeded into a 96-well plate at a density of  $5 \times 10^3$  per well and cultured overnight in normal RPMI-1640 culture medium with 10% fetal bovine serum (FBS) and 1% penicillin–streptomycin at 37 °C under 5% CO<sub>2</sub>. Then, the cells were washed with PBS and incubated with 100  $\mu$ l PAIONs in culture medium at various Fe concentrations (0–32.60  $\mu$ g Fe mL<sup>-1</sup>) at 37 °C for 12 h or 24 h. Afterwards, 20  $\mu$ l of 5 mg mL<sup>-1</sup> MTT [3-(4,5-dimethylthiazol-2-yl)-2,5-diphenyltetrazolium bromide] was added and allowed by incubation with the cells for 4 h. The culture medium was then removed before the addition of 150  $\mu$ l DMSO for dissolution of the precipitation. Finally, the absorption of each solution was measured at 570 nm on a SpectraMax M2 microplate reader (SpectraMax M2, Molecular Device, USA).

### *In vivo* MR imaging

Maintenance and care of all experimental animals used in the current study were carried out according to guidelines of IACUC of Tsinghua University, Beijing, China. Balb/C mice, with the average weight of 20 g and Japanese white rabbits, each weighing approximately 2 kg, were provided by the Beijing Center for Disease Control and Prevention (Beijing, China). Animals were maintained in SPF animal house under a 12 h light and 12 h darkness cycle and were fed a standard laboratory diet and tap water ad libitum. *In vivo*  $T_2$ -weighted MR images of mice were obtained by the following procedure. Mice were imaged using a temporomandibular joint coil on a 1.5 T MRI scanner. 12 nm PAION solution was intravenously injected *via* tail vein. The measurement parameters were as follows: echo train length (ETL) = 16, TR = 4000 ms, TE = 95.54 ms, FOV = 120 × 120 mm<sup>2</sup>, slice thickness per gap = 1.00 mm/0.5 mm and NEX = 6.

*In vivo*  $T_1$  and  $T_2$ -weighted MR images of rabbits were obtained by the following procedure: rabbits were imaged using a head coil on a 3 T MRI scanner. After the acquisition of pre-injection images, a dose of 1 mg Fe per kg of the 12 nm PAIONs was intravenously injected *via* ear vein. The measurement parameters of  $T_1$ -weighted image were as follows: ETL = 16, TR = 4 ms, TE = 2 ms, FOV = 325 × 325 mm<sup>2</sup>, slice thickness/gap = 1.6 mm/0.8 mm and NEX = 6. The measurement parameters of  $T_2$ -weighted image were as follows: ETL = 16, TR = 1000 ms, TE = 80 ms, FOV = 239 × 239 mm<sup>2</sup>, slice thickness/gap = 3.0 mm/1.0 mm and NEX = 6.

### Inductive heating property of MNPs under AMF

The magnetic heating system (SPG-06-II, Shenzhen Shuangping) was used to produce an alternating magnetic field with  $f = 526$  kHz and  $\mu_0 H_{\max} = 17.6$  mT. 5 mL PAION solution with iron concentration of 1 mg mL<sup>-1</sup> in a plastic test tube was placed in a foamed plastic thermal insulating support inside the coil for inductive heating property measurement. The temperature was measured with a FOT-301 fluoro-optic fiber thermometer (Xi'an

HeQi). The specific absorption rate (SAR) is determined by the following equation:

$$\text{SAR} = \frac{\sum_i C_i m_i}{m_{\text{Fe}}} \times \frac{\Delta T}{\Delta t}$$

where  $C_i$  is the specific heat of the different species in solution,  $m_i$  is the weight,  $m_{\text{Fe}}$  is the total mass of the iron and  $\Delta T/\Delta t$  is the slope of the  $T(t)$  curve.

## Results and discussion

To prepare monodispersed oleic acid (OA) stabilized 12 nm high-quality magnetite NPs with sphere shape, a solvothermal method was used. The high reaction pressure and relatively long reaction time are beneficial to produce high quality NPs. We also prepared 5 nm OA-stabilized iron oxide NPs by thermo-decomposition of iron oleate and 25 nm oleylamine (OAm)-stabilized iron oxide nanoprisms using the solvothermal method to examine the effectiveness of the ligand-exchange process for different types of MNPs.

Catechol derivatives, especially dopamine, are well explored as a binding anchor linking the inorganic surface and organic molecule. The high affinity to the inorganic surface will also allow ligands containing catechol derivatives to substitute the original surfactant and lots of successful examples have been reported.<sup>30,35,41</sup> However, considering the poor solubility of common catechol derivatives in non-polar or weak polar solvents, long-time heterogeneous reaction or further modification is required. To find a simple and rapid ligand-exchange method, we chose PA, which is commercially available, as a ligand. As a catechol derivative, PA can be well acted as a robust anchor of MNPs due to the high binding ability between catechol groups and metal oxides. The carboxyl-group of PA enables the excellent stability of NPs in water.

With certain amount of pyridine, PA can easily be dissolved in toluene. As an organic base, pyridine could weaken the hydrogen bond between PA molecules by forming salts, which results in dissolution of PA in toluene. After adding the mixture into the toluene solution of hydrophobic OA-stabilized NPs, the nanoparticles would precipitate in less than 1 min, indicating that the ligand exchange occurred rapidly (Fig. 1). The product after adding the mixture solution, which contains the pyridine salt, was not water soluble yet. Dilute alkaline solution was applied to remove pyridine, endow the NPs water solubility. This homogeneous ligand exchange method is beneficial, compared with the heterogeneous reaction with NPs in organic

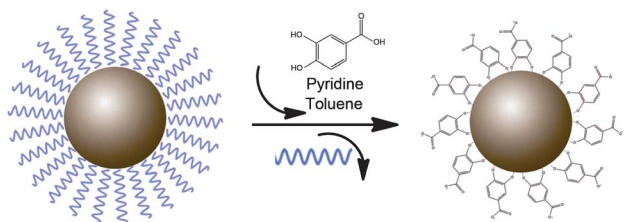


Fig. 1 Schematic illustration of the rapid ligand exchange process.

phase and the PA salt in water phase, with duration more than six hours was required for completing the ligand-exchange process. It is also a universal protocol, which can modify iron oxide NPs with different surfactant and preparation methods. To prove this, we also applied the method to iron oxide NPs coated with OA or OAm, and prepared by the thermo-decomposition or solvothermal method.

To confirm the ligand exchange mechanism, ATR-FTIR was used to explore the surface status of the MNPs before, during and after the ligand-exchange process of 12 nm OA-stabilized NPs (Fig. 2). For the NPs before the process, the peaks at 2923 and 2857  $\text{cm}^{-1}$  can be attributed to the presence of a hydrocarbon chain of the surfactant while the peaks at 1535 and 1427  $\text{cm}^{-1}$  indicate the anti-symmetric and symmetric vibration modes of the carboxyl group of fatty acid.<sup>38</sup> After addition of PA solution, the IR patterns of the precipitation of MNPs changed a lot. The peaks of C-H bond and carboxyl group of fatty acid disappeared and a new peak at 3259  $\text{cm}^{-1}$  appeared. The peak can be assigned to the vibration of the hydrogen bond of carboxyl hydrogen and pyridine. The peak at 1191 and 1103  $\text{cm}^{-1}$  can be assigned to the carboxyl and phenolic hydroxyl groups of PA. After the ligand-exchange, the obtained water-soluble NPs still showed the peaks of carboxyl and phenolic hydroxyl groups at 1265 and 1118  $\text{cm}^{-1}$  but the peak of the hydrogen band disappeared due to the removal of the pyridine.

Fig. 3a refers to TEM images of OA-stabilized MNPs prepared by the solvothermal method. The MNPs exhibited sphere morphology and narrow size distribution with an average diameter of about 12 nm. The inset is a photograph of hexane solution of OA-stabilized NPs with a lower layer of water. The dark hexane layer and the clear water layer indicate that the black OA-stabilized magnetite NPs had good solubility in a non-polar solvent and poor solubility in water. After ligand

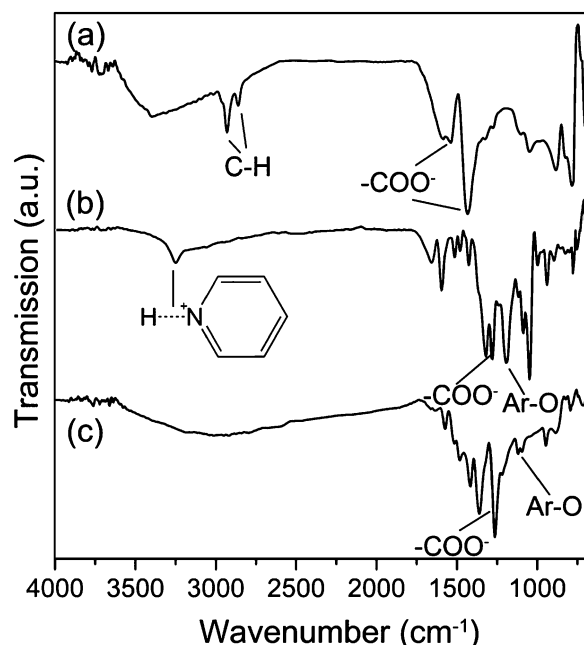
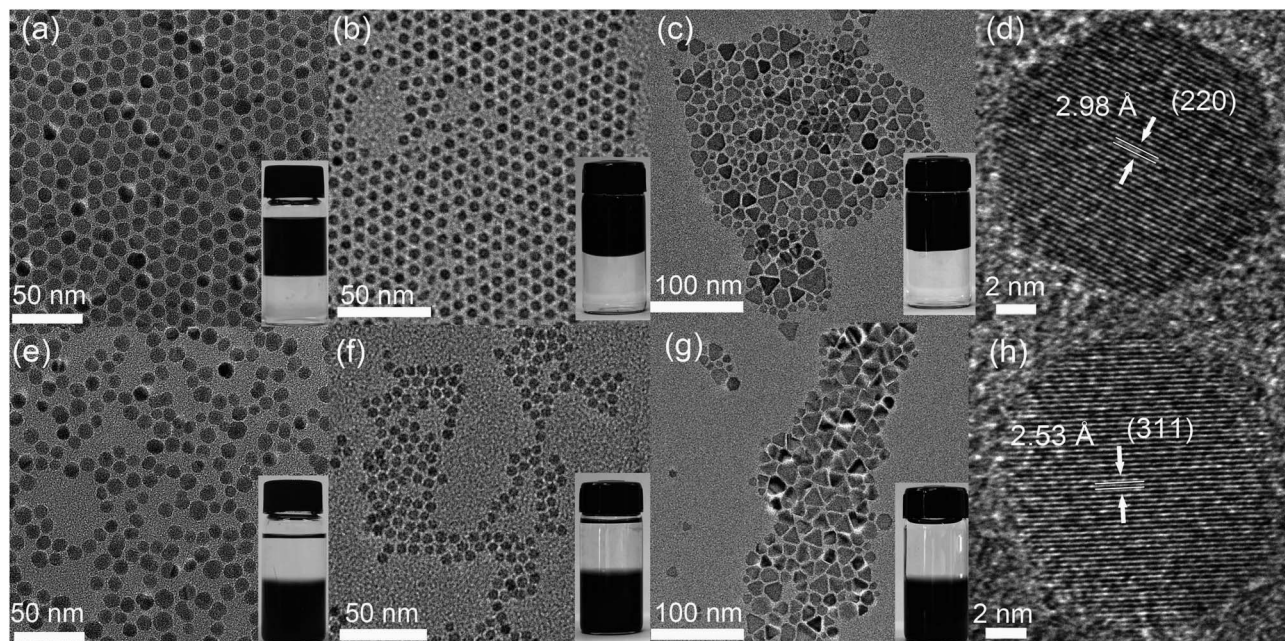


Fig. 2 FT-IR spectra of 12 nm magnetite nanoparticles (a) before, (b) during and (c) after ligand exchange.



**Fig. 3** (a–c and e–g) TEM images of iron oxide NPs: (a) 12 nm OA-stabilized NPs, (b) 5 nm OA-stabilized NPs, (c) 25 nm OAm-stabilized nanoprisms, (e) 12 nm PAIONS, (f) 5 nm PAIONS, and (g) 25 nm PAIONS. The insets in (a)–(c) show the corresponding photographs of the hydrophobic iron oxide NPs dispersed in hexane, with the lower layer of water; the insets in (e)–(g) show the corresponding photographs of the hydrophobic iron oxide NPs dispersed in hexane, with the lower layer of water; the insets in (e)–(g) show the corresponding photographs of the hydrophobic iron oxide NPs dispersed in water, with the upper layer of hexane. (d) and (h) HRTEM images of 12 nm magnetite NPs (d) before and (h) after ligand exchange.

exchange, the PAIONS showed a similar sphere morphology, size distribution and average diameter with corresponding OA-stabilized NPs and no aggregation was observed (Fig. 3e). The inset of Fig. 3e shows the photograph of black water solution of PAIONS with upper clear layer of hexane, indicating that the NPs had been successfully transferred to water by ligand exchange.

Fig. 3b and c show monodispersed 5 nm iron oxide NPs prepared by a thermo-decomposition method with OA as the stabilizer and 25 nm-sized iron oxide nanoprisms prepared by the solvothermal method with OAM as the stabilizer. The Fig. 3f and g are TEM images of the corresponding water-soluble NPs after ligand exchange, indicating no morphology change of the NPs. The insets of Fig. 3b and c show the photographs of hexane solution of hydrophobic NPs with the lower layer of water, while the insets of Fig. 3f and g show photographs of water solution of NPs after ligand-exchange with an upper layer of hexane. These series results revealed the PA-based ligand exchange protocol could obtain water-soluble NPs from the different types of hydrophobic ones without size and shape changes.

The influence of the ligand-exchange protocol on the fine-structure of the 12 nm NPs was further explored by high resolution transition electron microscopy (HRTEM). The OA-stabilized NPs showed single-crystal structure and the lattice spacing of 2.98 Å could be assigned to the (220) planes of magnetite (Fig. 3d). As depicted in Fig. 3h, single-crystal structure and lattice spacing could also be observed in PAION samples with lattice spacing of 2.53 Å ((311) planes of magnetite). Also, the crystallinity and fine structures of the NPs were not affected by the ligand exchange. The polycrystalline structure of magnetite NPs would induce reduction of magnetization

due to spin canting, spin glass or anti-phase boundary effects,<sup>42</sup> so the single crystal structure of PAIONS would benefit high magnetic performance.

It is important for ligand-exchange methods to avoid oxidation during the process and keep the original crystal structure and chemical composition of the NPs. Magnetite ( $\text{Fe}_3\text{O}_4$ , 92  $\text{emu g}^{-1}$ ) and maghemite ( $\gamma\text{-Fe}_2\text{O}_3$ , 76  $\text{emu g}^{-1}$ ) have similar inverse spinel type structure. The similarity of the structure allows easy transformation from magnetite to maghemite by oxidation, which would reduce the magnetic performance.

X-ray diffraction (XRD) analysis revealed that the 12 nm magnetite samples before and after ligand-exchange had identical patterns (Fig. 4a and b), which are in accord with pure face-centered cubic magnetite (JCPDS no. 65-3107). The average diameter of 13 nm was determined by the Scherrer equation:

$$D = K\lambda/\beta \cos \theta$$

where  $K$  is a constant,  $\lambda$  is the wavelength,  $\beta$  is the half-width, and  $\theta$  is the peak angle. The results were consistent with the TEM results. X-ray photoelectron spectroscopy (XPS) spectra were used to confirm the composition and valence state of the samples (Fig. 4c and d). The 12 nm OA-stabilized NPs showed two peaks at 710.26 eV and 724.20 eV, which are in accord with pure magnetite by comparing with the standard spectrum (710.29 eV and 724.09 eV). After ligand-exchange, the PAIONS presented two peaks at 710.31 eV and 724.50 eV, with little shift compared to the former sample, indicating the similar chemical composition. The XRD and XPS confirmed that both of the OA-stabilized NPs and PAIONS are  $\text{Fe}_3\text{O}_4$ . Because rapid reaction

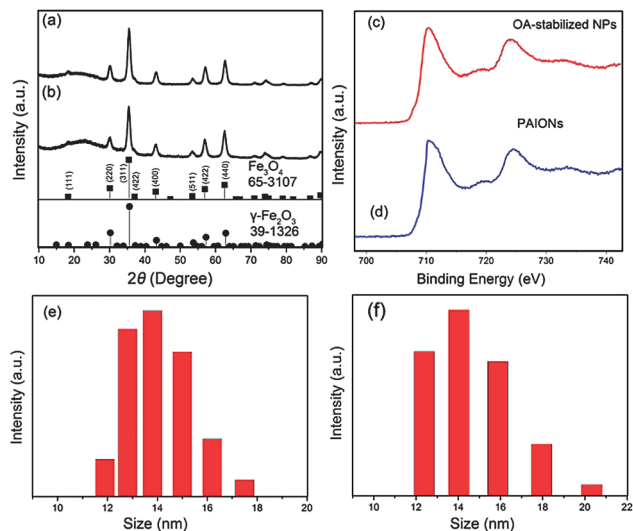


**Fig. 4** (a) and (b) XRD patterns of 12 nm magnetite NPs (a) before and (b) after ligand exchange. (c) and (d) XPS spectra of 12 nm magnetite NPs (c) before and (d) after ligand exchange. (e) and (f) DLS results of 12 nm PAIONs in (e) water and (f) PBS.

time avoids long time exposure to air for iron oxides during the reactions, the ligand-exchange process would not cause the oxidation of Fe<sub>3</sub>O<sub>4</sub>, leading to high quality water soluble iron oxide NPs.

The PA ligand was applicable to maintain the size of MNPs after ligand-exchange and avoid aggregation. Dynamic light scattering (DLS) was used for measuring the hydrodynamic size of PAIONs in water and PBS. As shown in Fig. 4e and f, the hydrodynamic size of PAIONs both in water and 1 × PBS was about 14 nm, very close to the TEM and XRD results. Moreover, the narrow size distribution is also desirable. Hydrodynamic size is an important parameter of water soluble NPs, especially for the NPs in biomedical applications. Considering the distance between the contrast agents and that water protons have great influence on their performance, small hydrodynamic size would be better for the application.

Commonly, a highly concentrated solution of well-dispersed MNPs with a long-chain stabilizer in a non-polar solvent, which could be considered as a ferrofluid, will exhibit strong response to an external magnetic field. However, plenty of hydrophilic groups cannot provide enough repel force, which will result in magnetic induced aggregation. As illustrated in Fig. 5, hexane solution of OA-stabilized 12 nm MNPs (10 mg mL<sup>-1</sup>) showed typical ferrofluidic behavior when the MNPs approached a magnet. The aqueous solution of 12 nm PAIONs with the same concentration exhibited a similar response to the magnetic field. After removal of the magnet, both of the solvents would return to a normal state, without any aggregation of NPs. Moreover, the NPs can remain stable for at least 6 months in an aqueous environment. The results indicate that the PA molecules are a strong ligand and stabilizer for magnetite NPs.

The magnetic property of the 12 nm magnetite NPs before and after ligand exchange was investigated by MPMS at room temperature with the magnetic field range of 0–5 T (0–50 kOe).



**Fig. 5** Photographs of the ferrofluidic behavior of 12 nm OA-stabilized NPs in hexane (left) and 12 nm PAIONs in water (right).

As shown in Fig. 6, OA-stabilized NPs exhibited typical superparamagnetic behavior. The inset depicts that the magnetization curve still crosses the origin even in the range of ±0.2 T, indicating that the sample had no coercivity and remanence. The saturation magnetization of the 12 nm OA-stabilized NPs was 66.5 emu g<sup>-1</sup>. Since the weight percentage of pure magnetite was 80% according to TGA analyses, the saturation magnetization at 5 T of the 12 nm magnetite NPs is 83 emu g<sup>-1</sup>, which is close to the value of MNPs with the similar size prepared by a high temperature thermo-decomposition method.<sup>25</sup> After ligand exchange, the 12 nm PAIONs showed a similar magnetization curve with the original one (Fig. 6b). The water soluble NPs were also superparamagnetic with saturation moment of 77.8 emu g<sup>-1</sup> (5 T). Despite little decrease in the value compared to the OA-stabilized NPs, the 12 nm PAIONs still expressed higher saturation magnetization than bulk γ-Fe<sub>2</sub>O<sub>3</sub>.

The magnetic performance of 5 nm OA-stabilized NPs and 25 nm OAm-stabilized nanoprisms before and after ligand exchange was investigated *via* PPMS at room temperature with magnetic field up to 3 T. All of the samples exhibited typical superparamagnetic behavior (Fig. 6c and d). However, even at 3 T, both OA and PA-stabilized NPs with 5 nm size showed

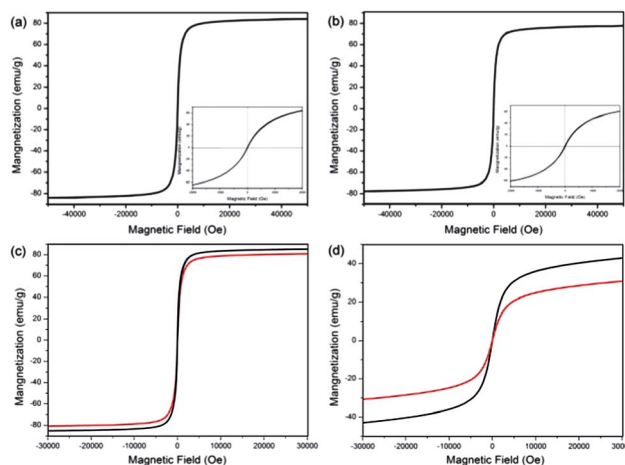


**Fig. 6** Field-dependent magnetization curves ( $M-H$ ) at 300 K for (a) 12 nm OA-stabilized magnetite NPs, (b) 12 nm PAIONs, (c) 25 nm nanoprisms before (black) and after (red) ligand exchange and (d) 5 nm NPs before (black) and after (red) ligand exchange. The insets in (a) and (b) show corresponding magnetization curves with a magnetic field range of 0–2000 Oe.

relatively low magnetic moment (Table 1), which can be attributed to oxidation and spin canting effects caused by large surface area.<sup>43,44</sup> In contrast, the 25 nm nanoprisms showed high magnetic performance. The transverse relaxivity of magnetic NPs as MR contrast agents is positively related to the square of their magnetic moment. Considering that the clinical MR system works at 1.5 or 3 T, the magnetic moment of the NPs is pivotal to the performance as  $T_2$  contrast agents. As listed in Table 1, both of the 12 nm and 25 nm PAIONs showed high magnetic moment close to the value of bulk magnetite indicating they are good candidate materials as  $T_2$ -weighted contrast agents.

To investigate the imaging properties of NPs, phantom experiments were performed using a 1.5 T clinical MR scanner. The 12 nm PAIONs showed longitudinal relaxivity ( $r_1$ ) of  $17.8 \text{ mM}^{-1} \text{ s}^{-1}$  and transverse relaxivity ( $r_2$ ) of  $220 \text{ mM}^{-1} \text{ s}^{-1}$  and the  $r_2/r_1$  ratio was about 12.4. The  $r_1$  of the agent is much higher than commercial Gd-DTPA ( $4.3 \text{ mM}^{-1} \text{ s}^{-1}$ )<sup>45</sup> and recently developed ESIONs ( $4.78 \text{ mM}^{-1} \text{ s}^{-1}$ ).<sup>14</sup> On the other side, the  $r_2$  result is compatible with bcc-Fe@Fe<sub>3</sub>O<sub>4</sub> NPs with PEG as a surfactant<sup>22</sup> and much better than commercial  $\gamma$ -Fe<sub>2</sub>O<sub>3</sub> based contrast agents, such as Feridex ( $120 \text{ mM}^{-1} \text{ s}^{-1}$ ).<sup>6</sup> Although it is commonly considered that when the  $r_2/r_1$  ratio is over 10, the contrast agent should be considered as the  $T_2$  contrast agent, there is no obvious influence on the  $T_1$  relaxation time by choosing appropriate imaging sequences.<sup>6</sup> In phantom experiments (Fig. 7), signals brightened in  $T_1$ -weighed images and darkened greatly in  $T_2$ -weighted images with the increase of iron concentration. The  $r_1$  and  $r_2$  of 5 nm PAIONs were 4.09 and  $17.7 \text{ mM}^{-1} \text{ s}^{-1}$  while the  $r_1$  and  $r_2$  of 25 nm PAIONs were 6.3 and  $233.7 \text{ mM}^{-1} \text{ s}^{-1}$ .

According to the quantum mechanical outer-sphere theory, the  $T_2$  relaxivity of magnetite NPs in aqueous solution can be obtained from the following equation:<sup>19</sup>

$$1/T_2 = (256\pi^2\gamma^2/405)V^*M_s^2\alpha^2/D(1 + L/\alpha)$$

where  $\gamma$  is the proton gyromagnetic ratio,  $V^*$  is the volume fraction,  $M_s$  is the saturation magnetization,  $\alpha$  is the radius of iron oxide core,  $D$  is the diffusivity of water molecules, and  $L$  is the thickness of an impermeable surface coating. Hence, 25 nm sized PAIONs, with very thin coating layer, high saturation magnetization and large radius of iron oxide core, are optimal for transverse relaxivity. However, due to the similar  $M_s$ , well modified 12 nm and PAIONs would also be a good candidate for  $T_2$ -weighted MRI contrast agent. On the other side, longitudinal relaxivity preferred to small size, which means the short distance between paramagnetic iron ions and protons in

**Table 1** Magnetization of the NPs before and after ligand exchange at various magnetic fields

	1.5 T (before) $\text{emu g}^{-1}$	3 T (before) $\text{emu g}^{-1}$	1.5 T (after) $\text{emu g}^{-1}$	3 T (after) $\text{emu g}^{-1}$
5 nm NPs	38.7	43	27.2	31.8
12 nm NPs	81.5	83	75	76.7
25 nm NPs	84.2	85.2	79.7	80.8

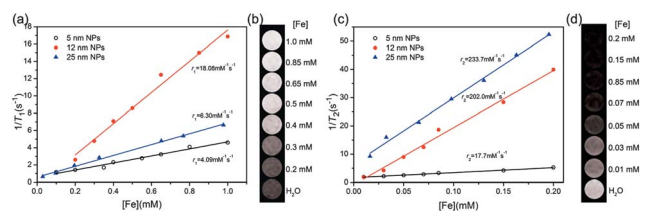


**Fig. 7** (a) Plot of  $1/T_1$  as a function of Fe concentration for PAIONs of 12 nm (dot), 25 nm (triangle), and 5 nm (circle). (b)  $T_1$ -weighted MR images of 12 nm PAIONs at different Fe concentrations. (c) Plot of  $1/T_2$  as a function of Fe concentration for PAIONs of 12 nm (dot), 25 nm (triangle), and 5 nm (circle). (d)  $T_2$ -weighted MR images of 12 nm PAIONs at different Fe concentrations.

water. The smaller sized 12 nm NPs, therefore, improve the longitudinal relaxivity tremendously. Despite the minor priority of 25 nm sized NPs in transverse relaxivity, considering both the longitudinal and transverse relaxivity, 12 nm PAIONs can be used as high performance dual-mode MRI contrast agent.

The cytotoxicity of the 12 nm PAIONs was evaluated *via* an MTT assay with HeLa cells, a kind of human cervical carcinoma cell line. For this study, HeLa cells were incubated with 0.25, 0.51, 1.02, 2.04, 4.08, 8.15, 16.30 or 32.60 mM Fe of the PAIONs for 12 h or 24 h. As shown in Fig. 8, after 12 h and 24 h incubation, the viabilities of HeLa cells were still >90% at all Fe incubation concentrations. These results demonstrated that the PAIONs showed little *in vitro* cytotoxicity, which indicated that they have potential for further *in vivo* applications.

To investigate the applicability for *in vivo* trials, the 12 nm PAIONs were first administered to mice and MRI experiments were performed at 1.5 T. Commonly, nanoscaled iron oxide-based contrast agent shows a strong tendency to accumulate in liver, spleen and lymph nodes, which are rich in phagocytic cells.<sup>46</sup> The contrast effect would help in the diagnosis of diseases in these organs, such as hepatocarcinoma. Fig. 9a–c show coronal  $T_2$ -weighted MR images of a control mouse and mice after intravenous administration of 12 nm PAIONs with 0.25 and 1 mg  $\text{kg}^{-1}$  Fe dose. Commonly, only when a Fe dose reaches 2.5 mg  $\text{kg}^{-1}$ , a good contrast effect would be achieved by using SPIO. But the liver was significantly darkened compared to the pre-injection figure even at the 0.25 mg  $\text{kg}^{-1}$  Fe

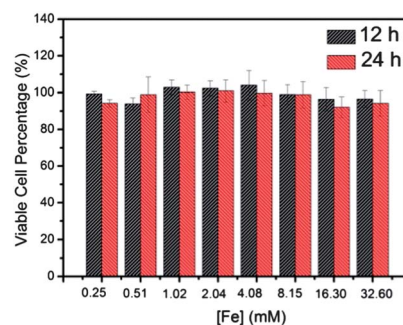


**Fig. 8** Cytotoxic effects of 12 nm PAIONs on HeLa cells treated with the MTT assay kit incubation with various concentrations of nanoparticles during 12 and 24 h incubation.

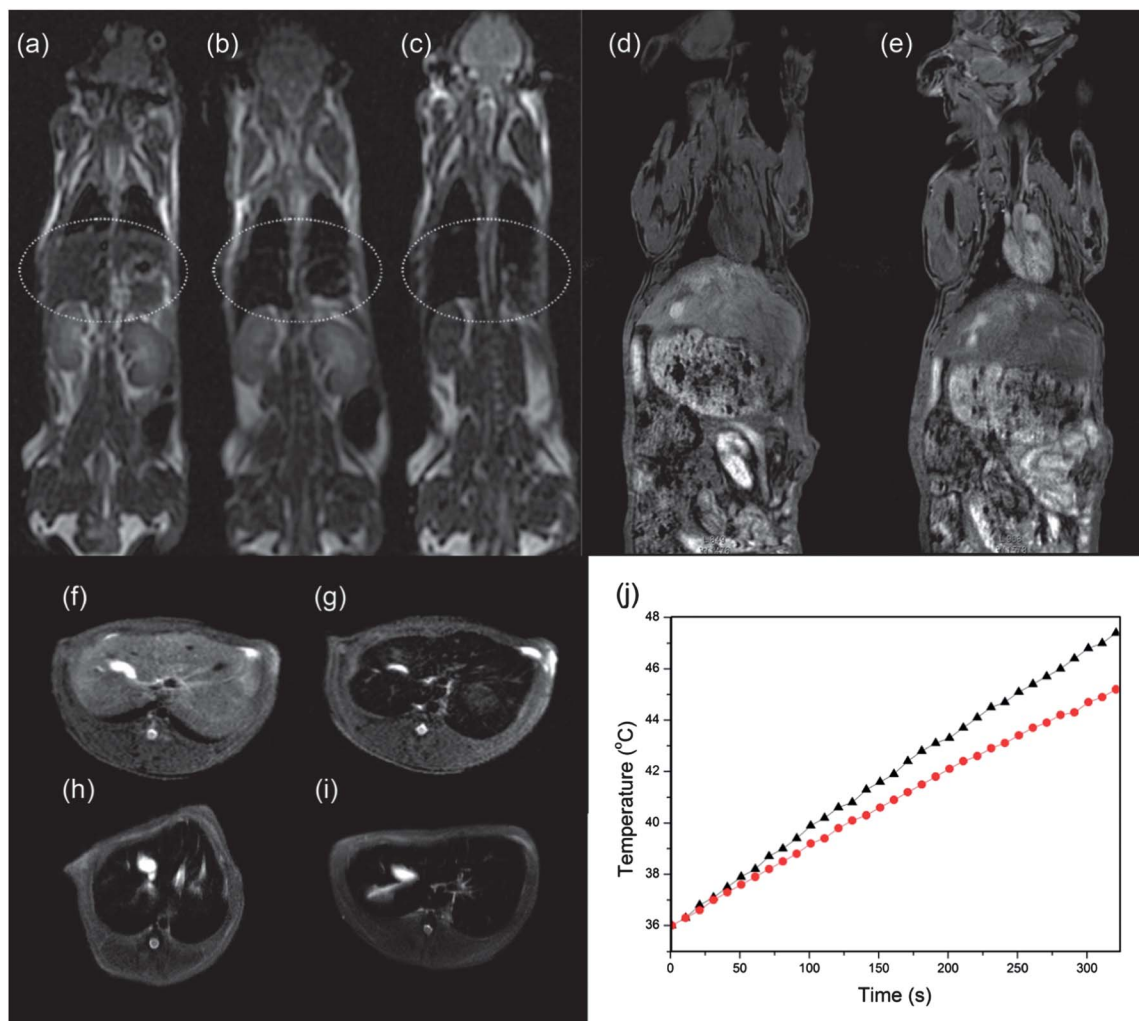


**Fig. 9** (a)–(c)  $T_2$ -weighted images of mouse (a) before and after injection of 12 nm PAIONs with a dose of (b)  $0.25 \text{ mg kg}^{-1}$  and (c)  $1 \text{ mg kg}^{-1}$  body weight. Circled area indicates liver. (d) and (e)  $T_1$ -weighted images of rabbit (d) before and (e) after injection of 12 nm PAIONs with a dose of  $1 \text{ mg kg}^{-1}$  body weight. (f)–(i)  $T_2$ -weighted images of rabbit (f) before injection and (g) 3 min, (h) 1 h or (i) 24 h after injection of 12 nm PAIONs with a dose of  $1 \text{ mg kg}^{-1}$  body weight. (j) Temperature profile during the hyperthermia experiment of 12 nm PAIONs (dot) and 25 nm PAIONs (triangle).

dose of PAIONs. The results suggested that the 12 nm PAION NPs can be excellent candidates for  $T_2$  contrast agents in MR imaging applications.

For better investigation their performance as dual mode contrast agents, further experiments of PAIONs were conducted on rabbits by using a Philips Achieva 3.0 T TX MR scanner. PAIONs were injected into a rabbit ( $1 \text{ mg Fe per kg}$ ) through its ear vein. The  $T_1$ -weighted image (Fig. 9e), which was acquired at 3 min after injection, showed a significant contrast enhancement of heart and blood vessels, indicating that 12 nm PAIONs can be used as good  $T_1$  MRI contrast agents. Fig. 9f–i show cross-sectional  $T_2$ -weighted images of the rabbit liver before and after intravenous administration of PAIONs. Comparing with the pre-injection image, the liver was completely darkened in 3 min, and still be darkened after 24 h. The study on mice and rabbit proved that PAIONs, which showed excellent *in vitro* longitudinal and transverse relaxivity, could also be used as good  $T_1$  and  $T_2$  dual-mode MRI contrast agent *in vivo*.

We evaluated the performance of PAIONs as magnetic hyperthermia agents. Fig. 9j depicts temperature profiles measured for the 12 nm and 25 nm PAIONs with iron concentration of  $1 \text{ mg mL}^{-1}$  under an alternating magnetic field. Both the samples could heat the aqueous solution from  $36^\circ\text{C}$  to  $46^\circ\text{C}$  within 5 min, which is high enough for tumor ablation. In contrast, the 5 nm PAIONs did not have heating effects. The specific absorption rate (SAR) is an important parameter for quantifying the heating efficiency of the NP. The SAR of the 12 nm PAIONs was  $26 \text{ W g}^{-1}$ , while the value of 25 nm PAIONs was  $31 \text{ W g}^{-1}$ . The SAR of PAIONs is suitable for magnetic hyperthermia. According to the Rosensweig model for super-paramagnetic NPs and the two relaxation mode (Néel relaxation and Brownian relaxation), the SAR of MNPs is determined by its coercivity, saturation magnetization, particle size and so on. The magnetite NPs we used showed high saturation magnetization but low coercivity, hence by using PAIONs produced from higher coercivity samples would show better magnetic heating property.

## Conclusions

We developed a rapid ligand-exchange process to produce high performance water-soluble iron oxide NPs by using commercially available low-toxic protocatechuic acid as a ligand and high quality hydrophobic NPs as start materials. The obtained PAIONs showed excellent water-solubility with very small hydrodynamic size in water or PBS. After ligand exchange, the crystal structure, chemical composition and magnetic property were well maintained. The 12 nm PAIONs exhibited saturation moment of 77.8 emu g<sup>-1</sup> and showed high MR relativities, which are nearly two times than commercial contrast agents. Such MNPs also possess ideal magnetic heating property. PAIONs can be high performance single compound multifunctional NPs as T<sub>1</sub> and T<sub>2</sub> multimodality MRI contrast agent and hyperthermia therapeutic agents. This PA-based ligand-exchange protocol not only provides a simple method for single compound multifunctional agents but also opens up a new possibility to water-soluble, biocompatible and high-performance iron oxide NPs for biomedical and other applications.

## Acknowledgements

This work was supported in part by the NSFC (51125001, 51172005, 90922033 and 21105120), the Natural Science Foundation of Beijing (2122022), the Doctoral Program of the Education Ministry of China (20120001110078) and PKU COE-Health Science Center Seed Fund.

## Notes and references

- 1 R. Hao, R. Xing, Z. Xu, Y. Hou, S. Gao and S. Sun, *Adv. Mater.*, 2010, **22**, 2729–2742.
- 2 H. B. Na, I. C. Song and T. Hyeon, *Adv. Mater.*, 2009, **21**, 2133–2148.
- 3 R. Weissleder and U. Mahmood, *Radiology*, 2001, **219**, 316–333.
- 4 D. Choi, A. Han, J. P. Park, J. K. Kim, J. H. Lee, T. H. Kim and S.-W. Kim, *Small*, 2009, **5**, 571–573.
- 5 K. H. Bae, Y. B. Kim, Y. Lee, J. Hwang, H. Park and T. G. Park, *Bioconjugate Chem.*, 2010, **21**, 505–512.
- 6 C. Corot, P. Robert, J. M. Idee and M. Port, *Adv. Drug Deliv. Rev.*, 2006, **58**, 1471–1504.
- 7 D. Yoo, J.-H. Lee, T.-H. Shin and J. Cheon, *Acc. Chem. Res.*, 2011, **44**, 863–874.
- 8 J.-s. Choi, J.-H. Lee, T.-H. Shin, H.-T. Song, E. Y. Kim and J. Cheon, *J. Am. Chem. Soc.*, 2010, **132**, 11015–11017.
- 9 G. K. Das, N. J. J. Johnson, J. Cramen, B. Blasiak, P. Latta, B. Tomanek and F. C. J. M. van Veggel, *J. Phys. Chem. Lett.*, 2012, **3**, 524–529.
- 10 M. J. Baek, J. Y. Park, W. Xu, K. Kattel, H. G. Kim, E. J. Lee, A. K. Patel, J. J. Lee, Y. Chang, T. J. Kim, J. E. Bae, K. S. Chae and G. H. Lee, *ACS Appl. Mater. Interfaces*, 2010, **2**, 2949–2955.
- 11 F. Hu, Q. Jia, Y. Li and M. Gao, *Nanotechnology*, 2011, **22**, 245604.
- 12 C. Kumar and F. Mohammad, *Adv. Drug Deliv. Rev.*, 2011, **63**, 789–808.
- 13 K. Hayashi, M. Nakamura, W. Sakamoto, T. Yogo, H. Miki, S. Ozaki, M. Abe, T. Matsumoto and K. Ishimura, *Theranostics*, 2013, **3**, 366–376.
- 14 B. H. Kim, N. Lee, H. Kim, K. An, Y. Il Park, Y. Choi, K. Shin, Y. Lee, S. G. Kwon, H. B. Na, J. G. Park, T. Y. Ahn, Y. W. Kim, W. K. Moon, S. H. Choi and T. Hyeon, *J. Am. Chem. Soc.*, 2011, **133**, 12624–12631.
- 15 S. Tong, S. Hou, Z. Zheng, J. Zhou and G. Bao, *Nano Lett.*, 2010, **10**, 4607–4613.
- 16 U. I. Tromsdorf, O. T. Bruns, S. C. Salmen, U. Beisiegel and H. Weller, *Nano Lett.*, 2009, **9**, 4434–4440.
- 17 J. W. M. Bulte and D. L. Kraitichman, *NMR Biomed.*, 2004, **17**, 484–499.
- 18 S. H. Koenig and K. E. Kellar, *Magn. Reson. Med.*, 1995, **34**, 227–233.
- 19 L. Lartigue, C. Innocenti, T. Kalaivani, A. Awwad, M. d. M. S. Duque, Y. Guari, J. Larionova, C. Guerin, J.-L. G. Montero, V. Barragan-Montero, P. Arosio, A. Lascialfari, D. Gatteschi and C. Sangregorio, *J. Am. Chem. Soc.*, 2011, **133**, 10459–10472.
- 20 R. E. Rosensweig, *J. Magn. Magn. Mater.*, 2002, **252**, 370–374.
- 21 P. Guardia, R. Di Corato, L. Lartigue, C. Wilhelm, A. Espinosa, M. Garcia-Hernandez, F. Gazeau, L. Manna and T. Pellegrino, *ACS Nano*, 2012, **6**, 3080–3091.
- 22 L.-M. Lacroix, N. Frey Huls, D. Ho, X. Sun, K. Cheng and S. Sun, *Nano Lett.*, 2011, **11**, 1641–1645.
- 23 W. S. Seo, J. H. Lee, X. M. Sun, Y. Suzuki, D. Mann, Z. Liu, M. Terashima, P. C. Yang, M. V. McConnell, D. G. Nishimura and H. J. Dai, *Nat. Mater.*, 2006, **5**, 971–976.
- 24 J. Park, K. An, Y. Hwang, J.-G. Park, H.-J. Noh, J.-Y. Kim, J.-H. Park, N.-M. Hwang and T. Hyeon, *Nat. Mater.*, 2004, **3**, 891–895.
- 25 S. Sun and H. Zeng, *J. Am. Chem. Soc.*, 2002, **124**, 8204–8205.
- 26 X. Wang, J. Zhuang, Q. Peng and Y. Li, *Nature*, 2005, **437**, 121–124.
- 27 Y. D. Yin, T. R. Zhang, J. P. Ge and Y. P. Hu, *Nano Lett.*, 2007, **7**, 3203–3207.
- 28 Y. I. Park, Y. Piao, N. Lee, B. Yoo, B. H. Kim, S. H. Choi and T. Hyeon, *J. Mater. Chem.*, 2011, **21**, 11472–11477.
- 29 R. De Palma, S. Peeters, M. J. Van Bael, H. Van den Rul, K. Bonroy, W. Laureyn, J. Mullens, G. Borghs and G. Maes, *Chem. Mater.*, 2007, **19**, 1821–1831.
- 30 H. B. Na, G. Palui, J. T. Rosenberg, X. Ji, S. C. Grant and H. Mattoussi, *ACS Nano*, 2012, **6**, 389–399.
- 31 Z. P. Chen, Y. Zhang, S. Zhang, J. G. Xia, J. W. Liu, K. Xu and N. Gu, *Colloids Surf., A*, 2008, **316**, 210–216.
- 32 N. Fauconnier, J. N. Pons, J. Roger and A. Bee, *J. Colloid Interface Sci.*, 1997, **194**, 427–433.
- 33 H. B. Na, I. S. Lee, H. Seo, Y. I. Park, J. H. Lee, S.-W. Kim and T. Hyeon, *Chem. Commun.*, 2007, 5167–5169.
- 34 E. Reimhult, E. Amstad, T. Gillich, I. Bilecka and M. Textor, *Nano Lett.*, 2009, **9**, 4042–4048.
- 35 J. Xie, C. Xu, N. Kohler, Y. Hou and S. Sun, *Adv. Mater.*, 2007, **19**, 3163–3166.

- 36 C. Xu, K. Xu, H. Gu, R. Zheng, H. Liu, X. Zhang, Z. Guo and B. Xu, *J. Am. Chem. Soc.*, 2004, **126**, 9938–9939.
- 37 A. S. Karakoti, S. Das, S. Thevuthasan and S. Seal, *Angew. Chem., Int. Ed.*, 2011, **50**, 1980–1994.
- 38 J. Ge, Y. Hu, M. Biasini, C. Dong, J. Guo, W. P. Beyermann and Y. Yin, *Chem.–Eur. J.*, 2007, **13**, 7153–7161.
- 39 H. Wei, N. Insin, J. Lee, H. S. Han, J. M. Cordero, W. Liu and M. G. Bawendi, *Nano Lett.*, 2012, **12**, 22–25.
- 40 Y. Zeng, R. Hao, B. Xing, Y. Hou and Z. Xu, *Chem. Commun.*, 2010, **46**, 3920–3922.
- 41 B. Xu, C. J. Xu, K. M. Xu, H. W. Gu, R. K. Zheng, H. Liu, X. X. Zhang and Z. H. Guo, *J. Am. Chem. Soc.*, 2004, **126**, 9938–9939.
- 42 M. Levy, A. Quarta, A. Espinosa, A. Figuerola, C. Wilhelm, M. García-Hernández, A. Genovese, A. Falqui, D. Alloyeau, R. Buonsanti, P. D. Cozzoli, M. A. García, F. Gazeau and T. Pellegrino, *Chem. Mater.*, 2011, **23**, 4170–4180.
- 43 S. Linderoth, P. V. Hendriksen, F. Bodker, S. Wells, K. Davies, S. W. Charles and S. Morup, *J. Appl. Phys.*, 1994, **75**, 6583–6585.
- 44 J. M. D. Coey, *Phys. Rev. Lett.*, 1971, **27**, 1140–1142.
- 45 P. Caravan, J. J. Ellison, T. J. McMurphy and R. B. Lauffer, *Chem. Rev.*, 1999, **99**, 2293–2352.
- 46 C. Corot, P. Robert, J.-M. Idee and M. Port, *Adv. Drug Deliv. Rev.*, 2006, **58**, 1471–1504.